Time-lapse monitoring of rock properties with coda wave interferometry

Alexandre Grêt,[1] Roel Snieder,[1] and John Scales[2]

Received 30 July 2004; revised 1 November 2005; accepted 21 November 2005; published 9 March 2006.

[1] The coda of seismic waves consists of that part of the signal after the directly arriving phases. In a finite medium, or in one that is strongly heterogeneous, the coda is dominated by waves which have repeatedly sampled the medium. Small changes in a medium which may have no detectable influence on the first arrivals are amplified by this repeated sampling and may thus be detectable in the coda. We refer to this use of multiple-sampling coda waveforms as coda wave interferometry. We have exploited ultrasonic coda waves to monitor time-varying rock properties in a laboratory environment. We have studied the dependence of velocity on uniaxial stress in Berea sandstone, the temperature dependence of velocity in granite and in aluminum, and the change in velocity due to an increase of water saturation in sandstone. There are many other possible applications of coda wave interferometry in geophysics, including dam and volcano monitoring, time-lapse reservoir characterization, earthquake relocation, and stress monitoring in mining and rock physics.

Citation: Grêt, A., R. Snieder, and J. Scales (2006), Time-lapse monitoring of rock properties with coda wave interferometry, *J. Geophys. Res.*, *111*, B03305, doi:10.1029/2004JB003354.

1. Introduction

[2] Geophysicists investigate the structure of the subsurface by making indirect measurements on the surface and relating them to those predicted by theoretical Earth models. The Earth, however, is a highly complex system, and we almost always have to simplify our models in order to make them tractable. In many applications, this simplification means treating unmodeled physics as noise, with the result that information contained in the data is discarded. For seismic data, this typically means ignoring the coda waves that make up the tail of a seismogram. (In music the coda is the concluding passage of a movement or composition (Latin cauda, tail).) Geophysical applications based on use of the coda waves include proposed schemes for earthquake prediction [*Aki*, 1985; *Sato*, 1988], volcano monitoring [*Poupinet et al.*, 1984; *Ratdomopurbo and Poupinet*, 1995; *Fehler et al.*, 1998; *Aki and Ferrazzini*, 2000] or monitoring of temporal changes in the subsurface [*Chouet*, 1979; *Revenaugh*, 1995; *Baisch and Bokelmann*, 2001; *Niu et al.*, 2003].

[3] Consider the following examples: in monitoring a nuclear waste disposal site, one is not primarily interested in imaging the site. It is, however, critical to monitor temporal changes in the site. In recent years, applied geophysicists have spent much effort on time-lapse seismology to monitor hydrocarbon reservoirs during recovery operations. Hydrocarbons move in the subsurface, reservoir rocks are artificially fractured, water-oil horizons move and injected steam propagates through the reservoir [*Lumley*, 1995; *Wang*, 1997]. The high sensitivity of coda waves to small perturbations of the medium makes them a powerful tool to monitor these kinds of changes.

[4] It is important to note that it is no more difficult to measure the coda energy than it is to measure first arrivals but we get additional information from the coda. Coda wave interferometry is one method to extract such information from the multiple scattered energy in the coda waves.

[5] We present four laboratory experiments in which we monitor the change in seismic velocity resulting from (1) a change in uniaxial stress in a sample of Berea sandstone, (2) a change in water saturation in a sample of Berea sandstone, (3) a temperature change in a sample of aluminum and (4) in a sample of Elberton granite. We excited and record ultrasonic waves to extract the velocity change from the coda waves.

2. Sensitivity of Coda Waves

[6] In a tomographic transmission experiment, the area under investigation is usually sampled once. The traversing waves have a certain sensitivity to a velocity change in this area (depending on distance, velocity and sampling). In a coincident source-receiver reflection experiment the area traversed by the waves is sampled twice and is therefore twice as sensitive to a velocity change than in the transmission case. Hence, in a setup where a wave is bouncing back and forth and samples the same area multiple times, the wave is much more sensitive to a velocity change. This

[1]Department of Geophysics, Center for Wave Phenomena, Colorado School of Mines, Golden, Colorado, USA.
[2]Department of Physics, Colorado School of Mines, Golden, Colorado, USA.

0148-0227/06/2004JB003354$09.00

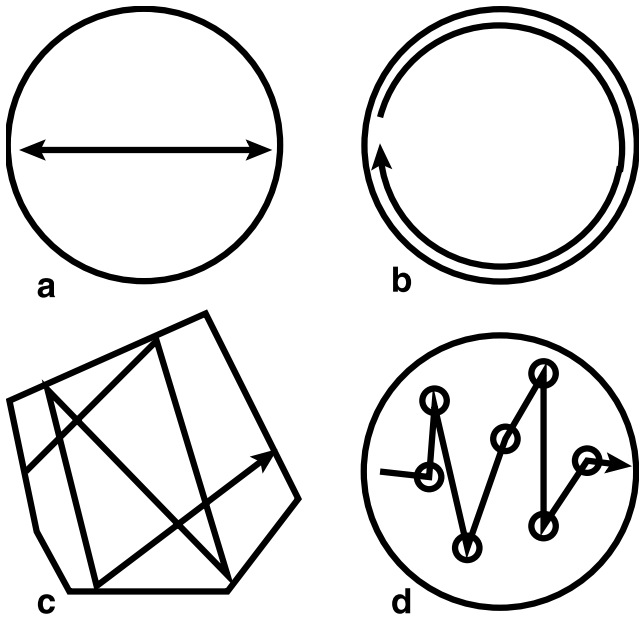

Figure 1. Cartoon of different wave modes that may coexist in a medium. (a) Bouncing ball mode where the waves go straight back and forth between two boundaries. (b) Surface waves that propagate along the boundary, circling the medium. (c) More complex reverberations between the boundaries. (d) Multiple scattering from small-scale scatterers (small circles) in the medium.

amplification of a velocity change due to the multiple sampling of the same area is the key idea we use in this research.

[7] Figure 1 outlines some examples of wave propagation where multiple sampling of the same area is achieved. In Figure 1a the waves bounce back and forth between opposite boundaries of the medium, we think of this as a "bouncing ball mode." In the laboratory experiment where we monitor a velocity change due to a change in uniaxial stress, we record a wave field which is dominated by such a bouncing ball mode (see section 4). In Figure 1b surface waves sample the medium by circling around the boundary, they are influenced by the velocity change each time they encircle the medium. Because of the cylindrical symmetry of the samples, surface waves dominate the coda in the experiment where we monitor temperature in aluminum and granite (see sections 6 and 7). In Figure 1c waves propagate in a more complex manner, bouncing off the boundaries in a complex pattern. Because of the irregular shape of the sandstone sample in the experiment where we monitor water saturation, we record such complex waveforms (see section 5).

[8] If the medium under investigation contains many small-scale scatterers, and the wave follows a path that connects these scatterers (Figure 1d), then the scattered path is much longer than the direct path from source to receiver. Hence the scattered wave is more sensitive to a velocity change than the direct wave. Examples of such scatterers in a background medium are colloidal suspensions, aerosols in air, and grains in rock.

[9] In a laboratory environment it is difficult to avoid waves that repeatedly sample the medium, because the samples are of finite size. The associated repeated sampling (as in Figure 1a) lends itself naturally to a modal (i.e., resonance) analysis, as shown for rock cores by *Scales and Malcolm* [2003]. Modal analysis is used in long-period seismology [e.g., *Dahlen and Tromp*, 1998] and resonance spectroscopy [*McSkimmin*, 1964; *Zadler et al.*, 2004]. The power of resonance comes from the ability to use frequency to selectively excite certain waves (e.g., a bouncing ball modes), and from Rayleigh's Principle [*Rayleigh and Strutt*, 1945, chapter 88] which states that the perturbation in the squared eigenfrequency of a mode can be related to perturbations in the density and elastic moduli, involving only the unperturbed mode vectors. *Zadler et al.* [2004] compare in detail the accuracy to which velocity changes can be measured with interferometry and with resonance spectroscopy. In field situations, however, there are scenarios where no modes can be excited (Figure 1d). In those situations, coda wave interferometry can still be applied as well as in the case where modes are excited.

[10] One can, of course, infer velocity changes as well from changes in the travel time of transmitted waves. We show several examples of changes in rock samples that give detectable changes in the coda waves, but that leave the first-arriving waves virtually unchanged. In an experiment with sufficient bandwidth, one can increase the sensitivity of time of flight measurements by increasing frequency. In practice, this is not always possible because of instrumental limitations, especially in field experiments, and because of attenuation. Time of flight measurements of the first-arriving waves provide a spatially localized measure of the velocity change. Since the coda waves sample the medium more globally than do the transmitted waves, coda wave interferometry gives a more global measure of the velocity change than does the transmitted wave. It depends on the goal of the experiment whether a local or a global measure of the velocity change in preferable.

[11] This sensitivity increase with longer path length is extensively used in optical applications, for example in atmospheric pollution analysis. In this application, air is introduced into a long tube. A laser pulse propagates trough the tube parallel to the long axis of the tube, and is measured at the other end. The ratio of the incident laser energy to the outgoing energy is a function of tube length, pollution density and pollution type. The longer the tube (path length), the more sensitive the instrument [*Hodges et al.*, 2004]. Similar to coda wave interferometry, the path can be increased by multiple sampling of the same area. In optics this is called cavity ring-down spectroscopy [*O'Keefe and Deacon*, 1988].

[12] The sensitivity also depends on signal-to-noise ratio, attenuation and dynamic range of the instrumentation [*Zadler et al.*, 2005]. Hence it might not always be possible to record coda waves because the signal-to-noise ratio is too small or the attenuation too large.

3. Estimation of Velocity Change From Coda Waves

[13] For a constant change δv in seismic velocity and fixed location of the scatterers and reflectors, we can write the propagation path $l = vt$, where v is the constant seismic velocity and t the propagation time. For a homogeneous

velocity change δv in the medium and an unchanged path we get $l = vt = (v + \delta v)(t + \delta t)$, or to first order

$$\frac{\delta v}{v} = \frac{-\delta t}{t}, \tag{1}$$

where δt is the travel time difference caused by the velocity change δv. A more rigorous derivation in given in Appendix A. We extract δt from the data by means of the cross-correlation function, where δt is given by the position of the maximum of the cross-correlation function that is defined as

$$R^{(t,t_w)}(t_s) \equiv \frac{\int_{t-t_w}^{t+t_w} u_{\mathrm{unp}}(t')u_{\mathrm{per}}(t'+t_s)dt'}{\left(\int_{t-t_w}^{t+t_w} u_{\mathrm{unp}}^2(t')dt' \int_{t-t_w}^{t+t_w} u_{\mathrm{per}}^2(t')dt'\right)^{\frac{1}{2}}}, \tag{2}$$

where the time window is centered at time t with duration $2t_w$, t_s is the time shift used in the cross correlation, u_{unp} is the unperturbed (before the velocity change) wave field and u_{per} the perturbed wave field.

[14] In the following experiments where we monitor rock properties, the coda consists of waves that are repeatedly reflected from the free surface, and waves scattered from the crystals and grains in rocks (see previous paragraph). The above formulation (equation (1), using the path summation in Appendix A), includes all the scenarios for multiple scattering sketched in Figure 1, and we can use the same theory for all our measurements.

[15] It is important to note that up to this point we have not distinguished between P or S waves. An extension for elastic waves is given by *Snieder* [2002], who uses an analysis based on a simple P and S wave equilibration model. *Snieder* [2002] shows that coda wave interferometry is much more sensitive to S wave than P wave velocity, in particular for a Poisson medium the velocity change measured with coda wave interferometry is given by

$$\frac{\delta v}{v} \approx 0.09\frac{\delta v_P}{v_P} + 0.91\frac{\delta v_S}{v_S}, \tag{3}$$

where v_S and v_P are S and P wave velocities, and δv_S and δv_P are the velocity changes for S and P waves, respectively. In some situations, the coda can be dominated by a modal behavior as sketched in Figure 1. In the case of a surface wave that repeatedly propagate around the circumference of a sample (Figure 1b), we measure a change in surface wave velocity, which is approximately 0.9 times the S wave velocity for typical rocks [*Carmichael*, 1982].

[16] In the following experiments we only consider the relative velocity change estimated from the coda of the ultrasonic measurements. Other types of perturbations such as the displacement of the source or receiver position and opening and closing of pores and fractures, leave a different signature on the time shifted correlation coefficient than a constant velocity change. Snieder *Snieder* [2004] gives a summary and a brief explanation for the different types of change that can be monitored with coda wave interferometry.

[17] All these laboratory experiments involve essentially the same measurement of ultrasonic waves, we measure the impulse response of a rock sample with compressional ultrasonic transducers. The difference between the experiments consists of the physics of the change introduced (stress, fluid saturation or temperature), the geometry, size and type (Berea sandstone, Elberton granite and aluminum) of the samples.

4. Monitoring Uniaxial Stress in Berea Sandstone

[18] Time-varying stress fields are important in a number of areas of geophysics. Changes near plate boundaries are important in order to understand plate tectonics [*Bokelmann and Silver*, 2002]. In earthquake prediction, the stress field is important for understanding fault behavior and its relation to earthquake occurrence [*Stein*, 1999; *Freed and Lin*, 2001; *Niu et al.*, 2003]. In hydrocarbon reservoirs, the stress field is changed by recovery operations. It is important to understand the associated temporal change for time-lapse reservoir monitoring [*Teanby et al.*, 2004]. In underground coal mining, "Room and Pillar" is a method in which approximately half of the coal is left in place to support the roof of the active mining area. Monitoring the stress field in the pillars and roofs is crucial for safe mining operations [*Nikitin*, 2003].

[19] *Wyllie et al.* [1958] measured ultrasonic P wave velocity as a function of effective stress in water-saturated Berea sandstone. They showed that at a constant confining pressure, v_p increases with decreasing pore pressure, and for constant effective stress the velocity remains approximately constant. Similar relationships between effective stress and P wave velocity have also been reported by others [e.g., *Nur and Simmons*, 1969; *Hicks and Berry*, 1956; *King*, 1966; *Christensen and Wang*, 1985]. Hence a good knowledge of seismic velocity is important for pore pressure prediction. Experimental results indicate that confining and pore pressures have almost equal but opposite effects on v_p (Terzaghi's effective stress principle). Confining pressure influences the wave velocities because pressure deforms most of the compliant parts of the pore space, such as microcracks and loose grain contacts. Closure of microcracks increases the stiffness of the rock and increases bulk and shear moduli. An increase in pore pressure mechanically opposes the closing of cracks and grain contacts, which lowers the effective moduli and velocities. Hence, when both confining pressure and pore pressures vary, only the difference between the two pressures has a significant influence on velocity [*Terzaghi*, 1936; *Hicks and Berry*, 1956].

[20] We show how coda wave interferometry can be used for stress field monitoring in a laboratory environment. In this experiment we use a fine-grained Berea sandstone to investigate the dependence of elastic waves on uniaxial stress. The sandstone block is equipped with an ultrasonic source (transducer) on one side and a receiver on the other (Figure 2). The transducer excites the rock with a pulse with a dominant frequency of 0.2 MHz. A single receiver records the propagated waves, with a sampling interval of 1 μs. To reduce the noise level, 512 traces are stacked for each stress level. A typical record is shown in Figure 3a.

[21] To introduce a controlled change in the medium over time, the sandstone block is placed in a hydraulic press and a uniaxial load is applied (see Figure 2). We monitor uniaxial load by a pressure sensor between rock and press.

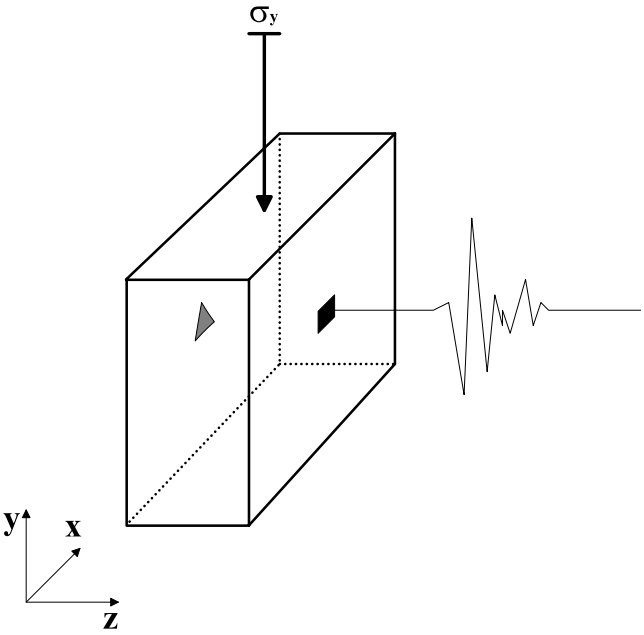

Figure 2. First experiment: A 12.5 × 40 × 40 cm^3 block of Berea sandstone is subjected to a uniaxial load in the *y* direction. Ultrasonic waves propagate in the *z* direction.

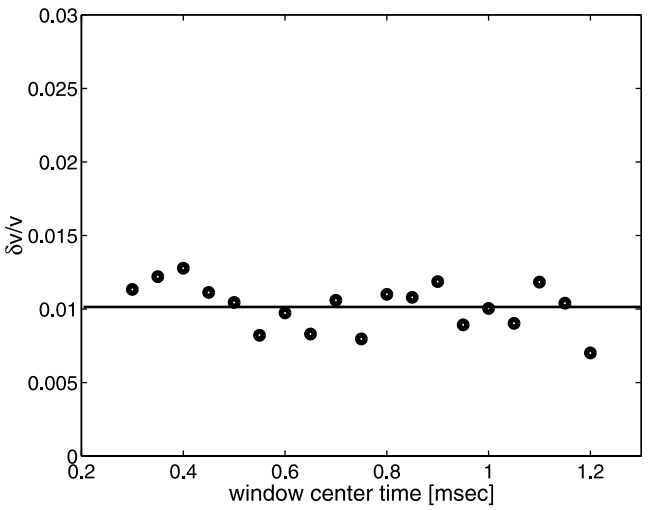

Figure 4. Velocity change estimates for 20 nonoverlapping windows with different center times. The mean velocity change is 1.02%, and the standard deviation is 0.16%.

For each stress state (4, 6 and 8 MPa) the ultrasonic measurement is repeated.

[22] Figure 3a shows two waveforms superimposed, one at a load of 6 MPa and the other at 8 MPa. After about 0.5 ms, the waves have a noisy appearance. If we look at a smaller time window as shown in Figure 3b, we see a strong correlation between the two waveforms, with one waveform time shifted with respect to the other. Thus despite the noisy appearance of the coda waves, these waves carry information about the structure of the medium, information that can be used to infer the change of sonic velocity with applied pressure.

[23] We infer the velocity change caused by an increase in the load from 6 MPa to 8 MPa, from the phase shift in the coda waves, using 20 nonoverlapping time windows each with a duration of 0.05 ms each of the coda waves, as described by *Snieder et al.* [2002]. The windows provide independent estimates of the relative velocity change. This can be used for a consistency check of the method. Since we have multiple estimates of $\delta v/v$ we can calculate the mean and variance of the relative velocity change. The relative velocity change for these time windows is shown in Figure 4, this change is of the order of 1.02% for a increase in load of 2 MPa with an error of 0.16%.

[24] *Sarkar et al.* [2003] shows comparable velocity changes in the same Berea sandstone block using one-way travel times of the first arrivals (1% for *P* waves and 3% for *S* waves). They estimate the uncertainty on the basis of errors in travel time picking to be approximately 1%. Note that their measured velocity change is on the same order of magnitude than the estimated uncertainty. The accuracy and sensitivity of coda wave interferometry are an order of magnitude higher than methods based on one-way travel time. In contrast to coda wave interferometry, *Sarkar et al.* [2003] are able to measure *P* and *S* wave velocity independently.

[25] Monitoring stress changes is important, for example, in mining applications, radioactive waste disposal cites or fault zones. Using coda wave interferometry in these

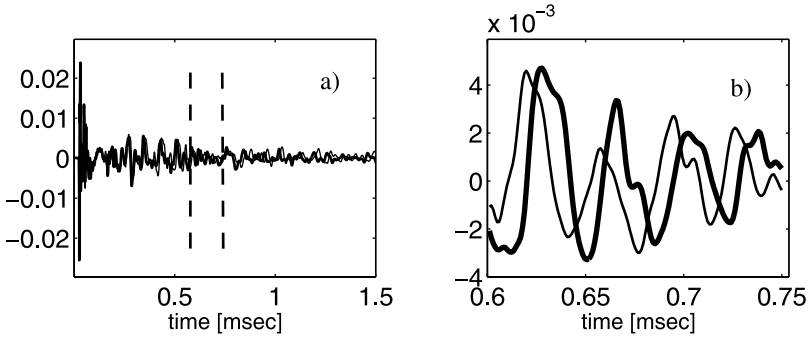

Figure 3. (a) Two waveforms recorded at an applied uniaxial load level of 6 MPa (thick line) and 8 MPa (thin line). (b) Same two waveforms as in Figure 3a, but only a small time window of the signal is shown; the time interval is marked by the two dashed lines in Figure 3a. The path length of the ultrasonic wave in this time interval is about 2.5 m, and the wave has bounced back and forth about 20 times.

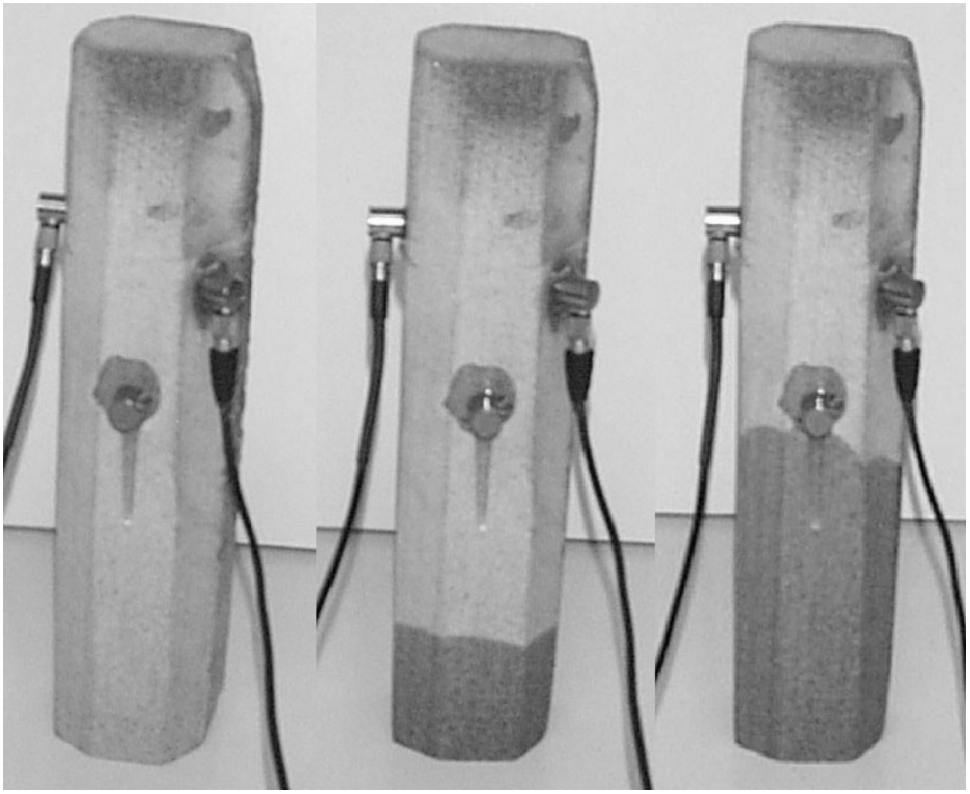

Figure 5. Berea sandstone sample as the fluid is infiltrating. Ultrasonic source and receiver are glued to the rock. The left picture shows the room-dry sample. The middle picture shows the water rising in the sandstone sample (dark line about a fourth of the way up the sample), and the right picture shows the water almost halfway up the rock. The third transducer glued to the rock is not used in this experiment.

applications could lead to a highly sensitive stress change monitoring technique with modest hardware requirements.

5. Monitoring Water Saturation in Berea Sandstone

[26] Seismic methods can monitor groundwater [*Bachrach and Nur*, 1998], dense nonaqueous phase liquid (DNAPL) contamination movement [*Griffin and Watson*, 2002], and hydrocarbon migration [*Lumley*, 1995; *Mjaaland et al.*, 2001] by detecting changes in seismic velocity. Compressional and shear wave velocities respond to changes in the bulk and shear modulus and density, caused by the presence of water. We demonstrate the application of coda wave interferometry for monitoring changes in water saturation in Berea sandstone.

[27] We use an irregularly shaped piece of Berea sandstone with an approximate height of 20 cm and an approximate diameter of 5 cm. The sample is equipped with a compressional source on one side and a receiver on the other (Figure 5). The room-dry sample is placed in a container that holds 5 mm of water. While the water is infiltrating into the pores of the sandstone by capillary pressure [*Wulff and Mjaaland*, 2002], the water level in the container is kept constant at 5 mm. When the water front is rising from 5 mm to 10 cm, we repeat the ultrasonic impulse response measurement for every 1 cm increase in water level in the sandstone. Again, for a 20 cm sample and a water front rise of 1 cm there is no significant travel time difference for the first arriving waves (see top inset of Figure 6). In a late time window (bottom inset of Figure 6), however, we see a distinct time shift of the waveforms.

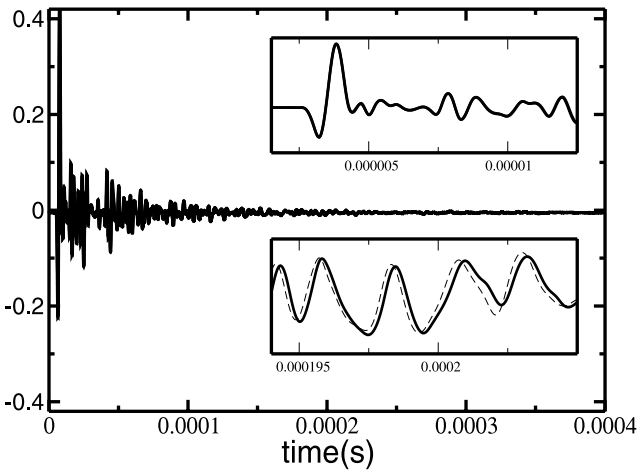

Figure 6. Waveforms recorded in the Berea sandstone block for two different levels of water saturation (water infiltrated 2 cm (dashed line) and 3 cm (solid line) of the rock). The insets show details of the waveforms (top) around the first arrival and (bottom) in the late coda. The dominant frequency is 0.33 MHz.

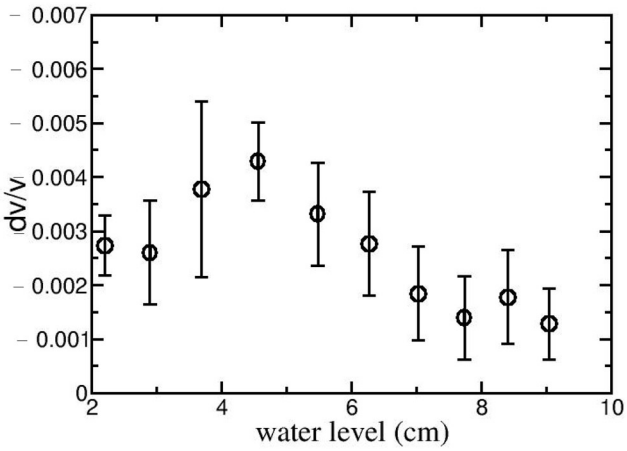

Figure 7. Relative velocity change $\delta v/v$ in Berea sandstone for approximately 1 cm increment in water level from room dry to 9 cm into the sample. Error bars are plus and minus one standard deviation.

[28] We infer the relative change in velocity for each change of 1cm in water level using 12 different 0.1 ms time windows of the coda waves. The relative velocity change is of the order of -0.3% for a water level rise of 1cm with an error of 0.05% (Figure 7). It is important to note that in many laboratory experiments, changes in rock properties are measured for saturation changes of about 5% on small samples [*Spencer*, 1981]. With coda wave interferometry we can monitor fluid saturation about 10 times more precisely.

[29] Figure 8 shows the consistent slowing of the sonic waves with increasing water level. However, in addition to the effect on velocity, fluid saturation changes the attenuation of the rock [*Mavko and Nur*, 1979]. In Figure 8 one can clearly see the amplitude decrease with increased water level. When monitoring velocity changes with coda wave interferometry, this attenuation change doesn't influence the estimates of the velocity change, because the normalization used in equation (2) renders the quantity independent of amplitude changes.

6. Monitoring Thermally Induced Velocity Changes in Aluminum

[30] The dependence of ultrasonic velocity on temperature in metals and alloys is an important characteristic in nondestructive testing [e.g., *Kobori and Iwashimizu*, 1990]. Often, the effect of stress on this velocity/temperature relationship is studied [*Salama and Ling*, 1980; *Chern and Heyman*, 1981]. Multiply scattered or reverberating waves are known to be sensitive to variations in temperature [*Weaver and Lobkis*, 2000]. We use this sensitivity of coda waves to monitor temperature changes in aluminum.

[31] In this ultrasonic experiment we use an aluminum cylinder with a height of 11 cm and a diameter of 5.5 cm. The sample is equipped with an ultrasonic source on one side and a receiver on the other (Figure 9). The transducer sends a pulse through the sample, and the single receiver records the impulse response of the sample, with a sampling interval of 1 μs (the dominant frequency is 100 kHz.) We stack ten traces to reduce the noise level. Two typical records for a cylindrical sample are shown in Figure 10. To apply a controlled change in the medium, the aluminum sample is equipped with a heating element in a central borehole. We monitor the temperature with two thermocouples glued to the side of the sample and in the borehole (Figure 9).

[32] While increasing the temperature from 25°C to 90°C, we repeat the ultrasonic measurement for every 5°C increase in temperature. Then the aluminum sample is cooled to room temperature and we repeat the ultrasound measurement again for every 5°C in temperature decrease.

[33] In some published laboratory experiments, the change in the seismic velocity is measured for a temperature change of about 100°C [*Timur*, 1977; *Peselnick and Stewart*, 1975; *Hughes and Maurette*, 1956]. For a 11 cm small sample and a temperature difference of only 5°C, there is no significant travel time difference for the first arriving waves (see top inset of Figure 10). Therefore first arriving waves do not provide any information about velocity changes for such a small temperature difference. In a late time window (bottom inset of Figure 10), we see a distinct time shift of the waveforms. This information can be used to infer the change of ultrasonic velocity with temperature.

[34] We estimate the relative change in velocity for each change of 5°C in temperature with 20 different 0.1 ms time windows of the coda waves (Figure 11). The relative velocity change is of the order of 0.15% for a temperature change of 5°C with an error of 0.025% (Figure 12). It is important to note that with the exception of a sign change, the relative velocity change with temperature does not depend on whether the sample is in the heating or the cooling phase. In other words, if we sum all the relative velocity changes for the heating phase (negative velocity change) and the cooling phase (positive velocity change) we obtain a relative velocity change after the heating cycle that is approximately zero.

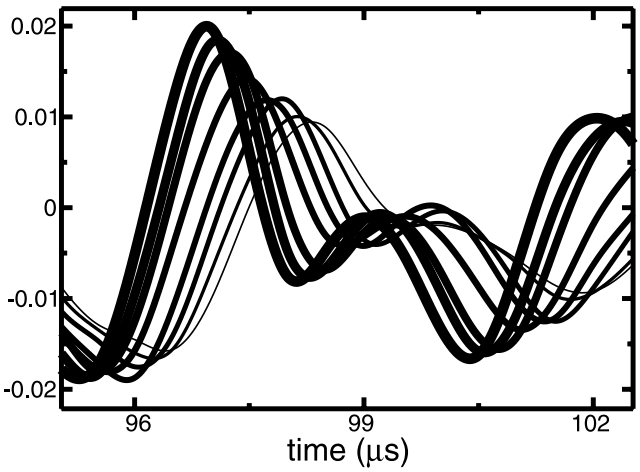

Figure 8. Eight waveforms, each measured at a different height of the water front. The fastest (thickest line) is measured on the dry sandstone, and the slowest (thinnest line) is measured at a water front height of 7 cm. In addition to the velocity change, the amplitudes decrease with increased water content in the sample.

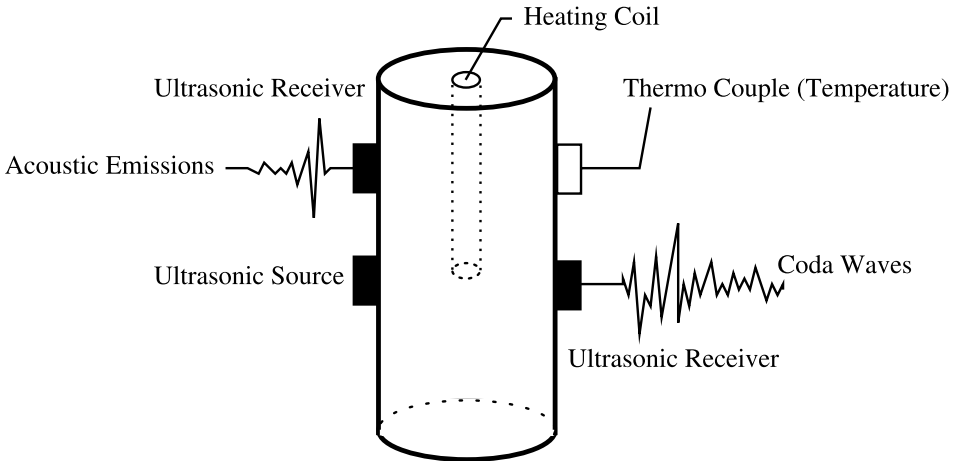

Figure 9. Cylinder representing the Elberton granite or the aluminum sample. Sonic waves are transmitted through the sample. A longitudinal transducer, which excites primarily P waves, and an identical receiver (bottom right rectangle) are used throughout the experiment. A third identical P wave transducer (top left rectangle) detects acoustic emissions. The sample is heated with a heating coil placed in a centered borehole, and the temperature is measured with a thermocouple at the sample surface (white rectangle.)

[35] We use this laboratory experiment to test the presence of nonlinear temperature effects on the measurement equipment, such as the piezoelectric transducers, the cables, the transducer couplant, and mounting devices. We measure a linear dependence of velocity on temperature in aluminum as in the experiment of *Weaver and Lobkis* [2000]. We therefore conclude that nonlinear instrument effects can be neglected. The change in path length due to thermal expansion of aluminum (10^{-5} C^{-1} [*Carmichael*, 1982]) causes an apparent velocity change. This effect is two orders of magnitude smaller than the obtained velocity change from the coda waves and can be neglected.

7. Monitoring Thermally Induced Velocity Change and Acoustic Emissions in Granite

[36] With the same technique and same experimental setup as described in the previous section, we measured the thermally induced velocity change in a granite sample. In addition, we count acoustic emissions for every temperature interval. Since the coefficient of thermal expansion for quartz is 10^{-6} C^{-1} [*Carmichael*, 1982], the associated apparent velocity change is three orders of magnitude smaller than the velocity change obtained from the coda waves and can be neglected.

[37] During the heating phase the velocity decrease (negative relative velocity change) is constant for each 5°C increase in temperatures, for temperatures below 70°C. At that temperature, however, the velocity change is nonlinear (Figure 13). Since we tested for nonlinear temperature effects of the measurement equipment on the aluminum sample, the nonlinear velocity decrease in granite must be attributed to a change in the rock sample. The temperature of 70°C corresponds to the critical fracture temperature for granite [*Johnson et al.*, 1978; *Fredrich and Wong*, 1986]. Thermal cracking results from the internal stress concentration induced by thermal expansion anisotropy or thermal expansion mismatch between minerals or grains. Such microcracking is a similar effect as the thermal stresses induced by thermal gradients in homogeneous solids; for a high temperature gradient, cracking may occur even in a perfectly homogeneous solid [*Boley and Weiner*, 1960]. *Fredrich and Wong* [1986] show that thermal cracking in rocks occurs principally along mineral or grain boundaries. The thermally induced cracks can significantly influence both the mechanical and transport properties, as well as thermoelastic moduli [*Simmons and Cooper*, 1978].

[38] In this experiment we use a third ultrasonic transducer to detect acoustic emissions in the granite due to thermal cracking. The histogram in Figure 13 shows the count of acoustic emissions versus temperature. There is a

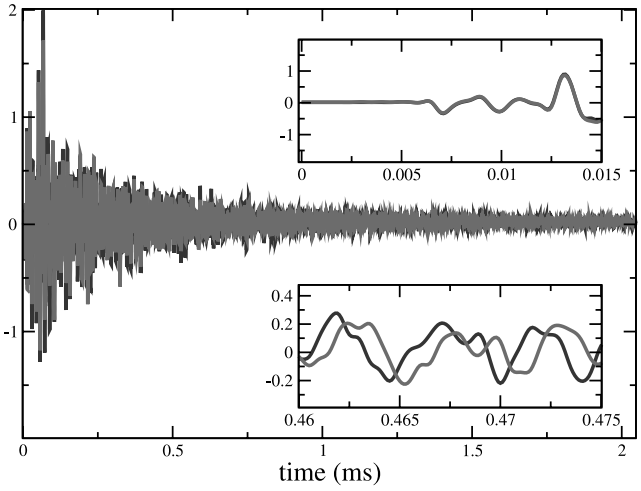

Figure 10. Waveforms recorded in the granite sample for temperatures of 45°C (gray line) and 50°C (black line). The insets show details of the waveforms (top) around the first arrival and (bottom) in the late coda. The main frequency in the data is 0.13 MHz.

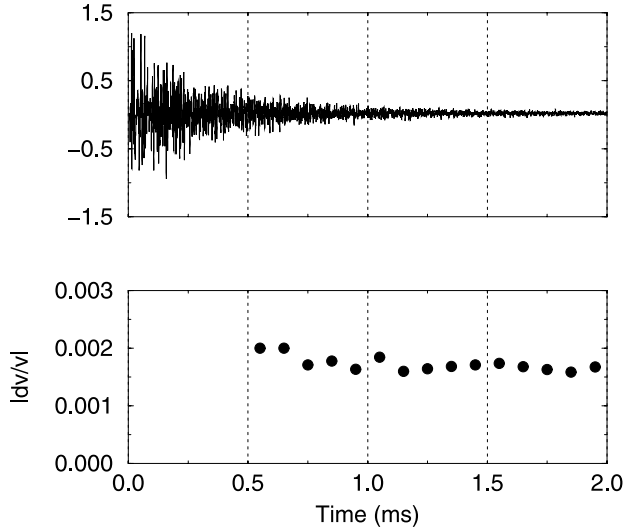

Figure 11. (top) Ultrasonic signal recorded on the aluminum sample. (bottom) Different estimates of $\delta v/v$ for multiple time windows, which provide a consistency check.

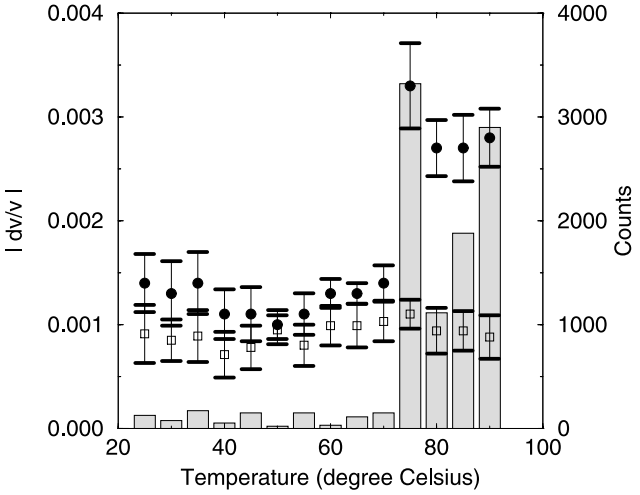

Figure 13. Absolute values of $\delta v/v$ in Elberton granite for 5°C temperature intervals from 25°C to 90°C. Circles correspond to the heating phase and rectangles to the cooling phase. The histograms show the count of acoustic emissions for a given temperature interval during the heating phase.

small number of acoustic emissions at low temperatures. There is, however, a significant increase in acoustic emissions between 70°C and 75°C. The increase in velocity change and the jump in the number of acoustic emissions correlate well.

[39] *Kaiser* [1953] found that during repeated loading of metals, little or no acoustic emissions occurred until previously applied stress levels where exceeded. Since then, this effect has been known as the ''Kaiser effect.'' Later, it was found that the Kaiser effect is a common phenomenon for various materials including rocks [*Kurita and Fujii*, 1979; *Lavrov*, 2002]. Thus the maximum stress applied in the previous cycles is 'memorized' in rocks.

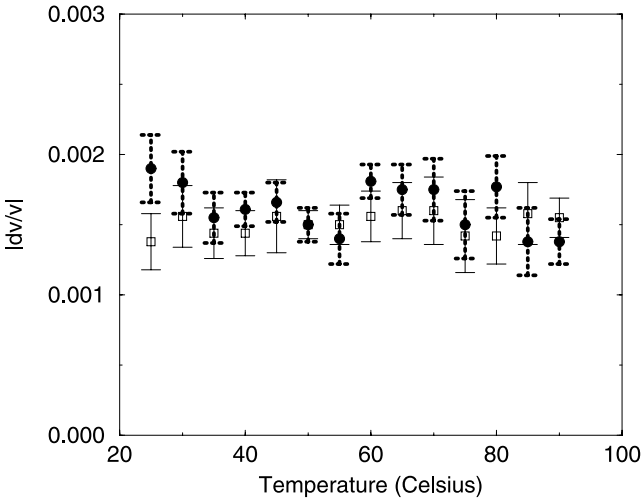

Figure 12. Absolute values of $\delta v/v$ in aluminum for 5°C temperature intervals from 25°C to 90°C. Solid circles correspond to the heating phase (velocity decrease) and open rectangles to the cooling phase (velocity increase).

[40] During the cooling phase of the granite, the velocity depends linearly on temperature over the whole temperature change and there are few acoustic emissions. The seismic velocity does not return to its initial value at the end of the cycle. This difference in velocity is due to irreversible damage done to the rock by thermal cracking (Figure 14).

[41] *Todd* [1973] studied the acoustic emissions of Westerly granite during cyclic heating. He noted that if a sample was reheated to the same maximum temperature, few acoustic emissions occurred. Similarly we find in a second heating cycle up to the same maximum temperature (90°C) for the same granite sample, only few acoustic emissions occur and there is no nonlinear velocity decrease around 70°C. Furthermore, the velocity increases back to the value before the second heating cycle when cooled down (Figure 14). Note that there is a small difference in relative velocity change between the cooling phase of the first heating cycle and the second cycle. *Thirumalai and Demou* [1973] studied the residual strain in a granitic rock produced by cyclic heating, and showed that predominant damage took place during the initial exposure to heating and the damage reached a steady state after three successive heating cycles. If we increase the temperature above the previous maximum temperature (90°C), the same nonlinear effect occurs; the granite ''remembers'' the maximum temperature.

[42] This indicates that two different mechanisms drive the temperature induced velocity change. The first mechanism is the change in bulk elastic constants with temperature, which is linear and reversible. This explains the constant velocity change with temperature during the second heating cycle during heating and cooling. The second mechanism is the irreversible damage done to the granite because of thermal cracking, which explains the nonlinear velocity change at the critical fracture temperature during the first heating cycle.

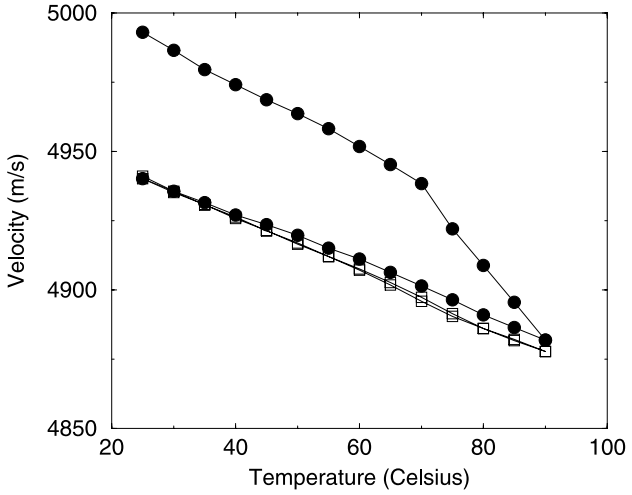

Figure 14. Velocity versus temperature in Elberton granite for two heating cycles. Solid circles represent the first heating cycle and open rectangles the second. Note that during the second heating cycle, the temperature-dependent velocities during the heating and cooling phase are indistinguishable.

[43] *Ide* [1937], found the same temperature dependence of velocity on temperature in Quincy granite. Using the travel time of first arrivals, he obtained 7 measurements over one heating cycle, with a peak temperature of 300°C. With coda wave interferometry we are able to measure twenty times more points over the same temperature interval. In other words, coda wave interferometry is orders of magnitude more sensitive to a temperature change.

8. Conclusions

[44] Because of the sensitivity of coda waves, we are able to study the influence of changes in stress, temperature and fluid on small samples to a high level of precision. The key idea is that multiple sampling of the same area increases the sensitivity of coda waves. This new level of sensitivity may lead to a better understanding of rock properties and material properties in general.

[45] The velocity estimation based on the coda waves requires only a single repeatable source and a single receiver, which makes it a potential method for inexpensive, real-time monitoring of land slides, hydrocarbon reservoirs, volcanoes, nuclear waste disposal sites and as a diagnostic tool in nondestructive testing. *Snieder and Vrijlandt* [2005] apply coda wave interferometry to obtain the relative location of earthquakes from the seismic coda.

[46] Coda wave interferometry has similarities with cavity ring-down spectroscopy [*O'Keefe and Deacon*, 1988] and resonance spectroscopy [*McSkimmin*, 1964]. In those methods modes are excited and analyzed in time or frequency. In contrast, we can use coda wave interferometry in field experiments, when it is not possible to excite modes because the system is open. For example, we use multiply scattered seismic waves to monitor a rapid temporal change in a volcano [*Grêt et al.*, 2005]. We could use coda wave interferometry to monitor minute changes in situ, for example in groundwater monitoring or DNAPL contamination. In addition there are countless industrial applications, where monitoring of stress, cracks, temperature and fluids is important, including aircraft engine monitoring, monitoring of punch press heads or applications in medical imaging like monitoring osteoporosis.

Appendix A: Brief Derivation of Coda Wave Interferometry

[47] This appendix follows *Snieder* [2002, 2006]. For a change in the wave velocity, for quasi-random perturbations of the point scatterer location, or for a change in the source location, we can estimate this perturbation from multiply scattered waves by a cross correlation in the time domain [*Snieder et al.*, 2002]. We refer to the waveform before the perturbation as the unperturbed signal, and to the waveform after the perturbation as the perturbed signal. The unperturbed wave field can be written as a Feynman path summation over all possible trajectories T [*Snieder*, 1999]:

$$u_{\mathrm{unp}}(t) = \sum_T A_T(t), \tag{A1}$$

where a trajectory is defined as a sequence of scatterers encountered by the wave. The sum over trajectories contains a sum over all possible mode conversions (P waves, S waves and surface waves), and it describes both trajectories that bounce off the free surface and/or trajectories that connect scatterers.

[48] When the background velocity is perturbed, the dominant effect on the waveform arises from the change in the travel time τ_T of the wave that travels along each trajectory:

$$u_{\mathrm{per}}(t) = \sum_T A_T(t - \tau_T). \tag{A2}$$

We can compute the time-windowed correlation coefficient between the unperturbed and the perturbed signal from equation (2). When the perturbed and unperturbed wave fields defined by equations (A1) and (A2) are inserted into (2), double sums over all trajectories appear. The cross terms with different trajectories ($T \neq T'$) are incoherent and average out to zero when the mean of the source signal vanishes. We therefore approximate the time-windowed correlation coefficient by

$$R^{(t,t_w)}(t_s) \approx \frac{\sum_{T(t,t_w)} C_T(\tau_T - t_s)}{\sum_{T(t,t_w)} C_T(0)}, \tag{A3}$$

where the sum is taken over the trajectories with arrival times within the time window of the cross correlation, and the autocorrelation of the source signal is defined as

$$C_T(t) \equiv \int_{-\infty}^{\infty} A_T(t' + t) A_T(t') dt'. \tag{A4}$$

[49] For time shifts τ much smaller than the dominant period, a second-order Taylor expansion gives $C(\tau)$ =

$C(0)(1 - \frac{1}{2}\overline{\omega}^2\tau^2)$, where $\overline{\omega}^2$ is the mean squared frequency of the waves that arrive in the time window defined as

$$\overline{\omega}^2 = -\frac{\sum_T \int_{t-t_w}^{t+t_w} A_T(t')\ddot{A}_T(t')dt'}{\sum_T \int_{t-t_w}^{t+t_w} A_T(t')^2 dt'}. \quad \text{(A5)}$$

Inserting the expansion (A1), ignoring cross terms ($T \neq T'$) and using an integration by parts this can be written as

$$\overline{\omega}^2 = \frac{\int_{t-t_w}^{t+t_w} u_{unp}^2(t')dt'}{\int_{t-t_w}^{t+t_w} u_{unp}^2(t')^2 dt'}. \quad \text{(A6)}$$

[50] Using this in equation (A3) we can write

$$R^{(t,t_w)}(t_s) = 1 - \frac{1}{2}\overline{\omega}^2 \left\langle (\tau - t_s)^2 \right\rangle_{(t,t_w)}, \quad \text{(A7)}$$

where $\langle \cdots \rangle_{(t,tw)}$ stands for the average over the wave paths with arrivals in the time interval $(t - t_w, t + t_w)$.

[51] The time-shifted cross correlation $R^{(t,tw)}(t_s)$ has a maximum when

$$t_s = t_{\max} \equiv \langle \tau \rangle_{(t,t_w)}, \quad \text{(A8)}$$

where $\langle \tau \rangle_{(t,tw)}$ is the mean travel time perturbation of the arrivals in the time window. Using expressions (A7) and (A8) gives the maximum value of the cross correlation

$$R_{\max}^{(t,t_w)} = 1 - \frac{1}{2}\overline{\omega}^2 \sigma_\tau^2, \quad \text{(A9)}$$

where σ_τ^2 is the variance of the travel time perturbation for waves arriving within the time window. This means that we can extract the mean and the variance of the travel time perturbations of the waves arriving in a time window.

[52] For a constant change δv in seismic velocity and fixed locations of the scatterers, the mean travel time perturbation is given by $\langle \tau \rangle_{(t,tw)} = -(\delta v/v)t$. When the time window is small ($t_w \ll t$), $\sigma_\tau \approx 0$. The velocity change follows from the time of the maximum of the time-shifted cross-correlation function

$$\frac{\delta v}{v} = \frac{-t_{\max}}{t}. \quad \text{(A10)}$$

[53] **Acknowledgments.** We thank Bob Kranz, Debashish Sarkar, and Mike Batzle for their help with the experiments. We also thank the members of the Center for Wave Phenomena and the Physical Acoustics Laboratory for stimulating discussions. This work was supported by the NSF (EAR-0106668 and EAR-0337379).

References

Aki, K. (1985), Theory of earthquake prediction with special reference to monitoring of the quality factor of lithosphere by the coda method, *Earthquake Res. Bull.*, *3*, 219–230.

Aki, K., and V. Ferrazzini (2000), Seismic monitoring and modeling of an active volcano for prediction, *J. Geophys. Res.*, *105*, 16,617–16,640.

Bachrach, R., and A. Nur (1998), High-resolution shallow-seismic experiments in sand, part I: Water table, fluid flow, and saturation, *Geophysics*, *63*, 1225–1233.

Baisch, S., and G. Bokelmann (2001), Seismic waveform attributes before and after the Loma Prieta earthquake: Scattering change near the earthquake and temporal recovery, *J. Geophys. Res.*, *106*, 16,323–16,337.

Bokelmann, G., and P. Silver (2002), Shear stress at the base of shield lithosphere, *Geophys. Res. Lett.*, *29*(23), 2091, doi:10.1029/2002GL015925.

Boley, B., and J. Weiner (1960), *Theory of Thermal Stresses*, 586 pp., Dover, Mineola, N. Y.

Carmichael, R. S. (1982), *Handbook of Physical Properties of Rocks*, CRC Press, Boca Raton, Fla.

Chern, C., and J. Heyman (1981), Determination of material stress from the temperature dependence of acoustic natural velocity, *Proc. IEEE Ultrason. Symp.*, 960–965.

Chouet, B. (1979), Temporal variation in the attenuation of earthquake coda near Stone Canyon, California, *Geophys. Res. Lett.*, *6*, 143–146.

Christensen, N., and H. Wang (1985), The influence of pore pressure and confining pressure on dynamic elastic properties of Berea sandstone, *Geophysics*, *50*, 207–213.

Dahlen, F. A., and J. Tromp (1998), *Theoretical Global Seismology*, Princeton Univ. Press, Princeton, N. J.

Fehler, M., P. Roberts, and T. Fairbanks (1998), A temporal change in coda wave attenuation observed during an eruption of Mount St. Helens, *J. Geophys. Res.*, *93*, 4367–4373.

Fredrich, J., and T. Wong (1986), Micromechanics of thermally induced cracking in three crustal rocks, *J. Geophys. Res.*, *91*, 12,743–12,764.

Freed, A., and J. Lin (2001), Delayed triggering of the 1999 Hector Mine earthquake by viscoelastic stress transfer, *Nature*, *411*, 180–183.

Grêt, A. A., R. Snieder, and R. Aster (2005), Monitoring rapid temporal change in a volcano with coda wave interferometry, *Geophys. Res. Lett.*, *32*, L06304, doi:10.1029/2004GL021143.

Griffin, T., and K. Watson (2002), A comparison of field techniques for confirming dense nonaqeuous phase liquids, *Ground Water Monit. Rem.*, *22*(2), 28–30.

Hicks, W., and J. Berry (1956), Application of continuous velocity logs to determination of fluid saturation of reservoir rocks, *Geophysics*, *21*, 739–744.

Hodges, J. T., H. P. Layer, W. W. Miller, and G. E. Scace (2004), Frequency-stabilized single-mode cavity ring-down apparatus for high-resolution absorption spectroscopy, *Rev. Sci. Instrum.*, *75*(4), 849–863.

Hughes, D., and C. Maurette (1956), Variation of elastic wave velocities in granites with pressure and temperature, *Geophysics*, *21*, 277–284.

Ide, J. (1937), The velocity of sound in rocks and glasses as a function of temperature, *J. Geol.*, *45*, 689–716.

Johnson, B., A. Gangi, and J. Handin (1978), Thermal cracking subjected to slow, uniform temperature changes, paper presented at 19th U. S. Rock Mechanics Symposium, U.S. Natl. Comm. for Rock Mech., Univ. of Nev., Reno.

Kaiser, J. (1953), Erkenntnisse und Folgerungen aus der Messung von Gerüschen bei Zugbeanspruchung von metallischen Werkstoffen, *Arch. Eisenhuettenwes.*, *24*, 43–45.

King, M. (1966), Wave velocities in rocks as a function of changes in overburden pressure and pore fluid saturation, *Geophysics*, *31*, 50–73.

Kobori, O., and Y. Iwashimizu (1990), Effects of stress and temperature on ultrasonic velocity, in *Elastic Waves and Ultrasonic Nondestructive Evaluation*, edited by S. K. Datta, J. D. Achenbach, and Y. Rajapakse, Elsevier, New York.

Kurita, K., and N. Fujii (1979), Stress memory of crystalline rocks in acoustic emission, *Geophys. Res. Lett.*, *6*, 9–12.

Lavrov, A. (2002), The Kaiser effect in rocks: Principles and stress estimation technique, *Int. J. Rock Mech. Min. Sci.*, *40*, 151–171.

Lumley, D. (1995), Seismic time-lapse monitoring of subsurface fluid flow, Ph.D. thesis, Stanford Univ., Stanford, Calif.

Mavko, G. M., and A. Nur (1979), Wave attenuation in partially saturated rocks, *Geophysics*, *44*, 161–178.

McSkimmin, H. J. (1964), Ultrasonic methods for measuring the mechanical properties of liquids and solids, in *Physical Acoustics*, vol. 1A, Edited by W. P. Mason, chap. 4, Elsevier, New York.

Mjaaland, S., E. Causse, and A. Wulddd (2001), Seismic monitoring from intelligent wells, *Leading Edge*, *20*, 1180–1184.

Nikitin, O. (2003), Mining block stability analysis for room-and-pillar mining with continuous miner in estonian oil shale mines, *Oil Shale*, *20*, 515–528.

Niu, F., P. Silver, R. Nadeau, and T. McEvilly (2003), Migration of seismic scatterers associated with the 1993 Parkfield aseismic transient event, *Nature*, *426*, 544–548.

Nur, A., and G. Simmons (1969), The effect of saturation on velocity in low porosity rocks, *Earth Planet. Sci. Lett.*, *7*, 183–190.

O'Keefe, A., and D. A. G. Deacon (1988), Cavity ring-down optical spectrometer for absorption measurements using pulsed laser sources, *Rev. Sci. Instrum.*, *59*(12), 2544–2551.

Peselnick, L., and R. Stewart (1975), A sample assembly for velocity measurements of rocks at elevated temperatures and pressures, *J. Geophys. Res.*, *80*, 3765–3768.

Poupinet, G., W. L. Ellsworth, and J. Frechet (1984), Monitoring velocity variations in the crust using earthquake doublets: An application to the Calaveras fault, California, *J. Geophys. Res.*, *89*, 5719–5731.

Ratdomopurbo, A., and G. Poupinet (1995), Monitoring a temporal change of seismic velocity in a volcano: Application to the 1992 eruption of Mt. Merapi (Indonesia), *Geophys. Res. Lett.*, *22*, 775–778.

Rayleigh, B., and J. W. Strutt (1945), *The Theory of Sound*, vol. 1, 2nd ed., Dover, Mineola, N. Y.

Revenaugh, J. (1995), The contribution of topographic scattering to teleseismic coda in southern California, *Geophys. Res. Lett.*, *22*, 543–546.

Salama, K., and C. Ling (1980), The effect of stress on the temperature dependence of ultrasonic velocity, *J. Appl. Phys.*, *51*, 1505–1510.

Sarkar, D., A. Bakulin, and R. L. Kranz (2003), Anisotropic inversion of seismic data for stressed media: Theory and a physical modeling study on Berea sandstone, *Geophysics*, *68*, 690–704.

Sato, H. (1988), Temporal change in scattering and attenuation associated with the earthquake occurence: A review of recent studies on coda waves, *Pure Appl. Geophys.*, *126*, 465–497.

Scales, J. A., and A. E. Malcolm (2003), Laser characterization of ultrasonic wave propagation in random media, *Phys. Rev. E*, *67*, 04,6618.

Simmons, G., and H. Cooper (1978), Thermal cycling cracks in three igneous rocks, *Int. J. Rock Mech.*, *15*, 145–148.

Snieder, R. (1999), Imaging and averaging in complex media, in *Diffuse Waves in Complex Media*, edited by J. Fouque, pp. 405–454, Springer, New York.

Snieder, R. (2002), Coda wave interferometry and the equilibration of energy in elastic media, *Phys. Rev. E*, *66*, 04,6615.

Snieder, R. (2004), Coda wave interferometry, in *2004 McGraw-Hill Yearbook of Science and Technology*, pp. 54–56, McGraw-Hill, New York.

Snieder, R. (2006), The theory of coda wave interferometry, *Pure Appl. Geophys*, in press.

Snieder, R., and M. Vrijlandt (2005), Constraining relative source locations with coda wave interferometry: Theory and application to earthquake doublets in the Hayward fault, California, *J. Geophys. Res.*, *110*, B04301, doi:10.1029/2004JB003317.

Snieder, R., A. Grêt, H. Douma, and J. Scales (2002), Coda wave interferometry for estimating nonlinear behavior in seismic velocity, *Science*, *295*, 2253–2255.

Spencer, J. W. (1981), Stress relaxation at low frequencies in fluid-saturated rocks: Attenuation and modulus dispersion, *J. Geophys. Res.*, *86*, 1803–1812.

Stein, R. (1999), The role of stress transfer in earthquake occurrence, *Nature*, *402*, 605–609.

Teanby, N., J. Kendall, R. Jones, and O. Barkved (2004), Stress-induced temporal variations in seismic anisotropy observed in microseismic data, *Geophys. J. Int.*, *156*, 459–466.

Terzaghi, K. (1936), The shearing resistance of saturated soils, paper presented at First International Conference on Soil Mechanics and Foundation Engineering, Int. Soc. of Soil Mec. and Found. Eng., Cambridge, Mass.

Thirumalai, K., and S. Demou (1973), Thermal expansion behaviour of intact and thermal fractured mine rocks, paper presented at 19th Annual American Institute of Physics Conference, Boston, Mass.

Timur, A. (1977), Temperature dependence of compressional and shear wave velocities in rocks, *Geophysics*, *42*, 950–956.

Todd, T. (1973), Effects of cracks on elastic properties of low porosity rocks, Ph.D. thesis, Mass. Inst. of Technol., Cambridge.

Wang, Z. (1997), Feasibility of time-lapse seismic reservoir monitoring: The physical basis, *Leading Edge*, *16*, 1327–1329.

Weaver, R., and O. Lobkis (2000), Temperature dependence of diffuse field phase, *Ultrasonics*, *38*, 491–494.

Wulff, A., and S. Mjaaland (2002), Seismic monitoring of fluid fronts: An experimental study, *Geophysics*, *67*, 221–229.

Wyllie, M., A. Gregory, and G. Gardner (1958), An experimental investigation of factors affecting elastic wave velocities in porous media, *Geophysics*, *23*, 459–494.

Zadler, J. B., A. Grêt, and J. A. Scales (2005), Spectroscopy versus interferometry: Resolving small changes, *Am. J. Phys.*, *73*, 837–844.

Zadler, B., J. LeRousseau, J. Scales, and M. Smith (2004), Resonance ultrasound spectroscopy: Theory and application, *Geophys. J. Int.*, *156*, 154–169.

A. Grêt and R. Snieder, Department of Geophysics, Center for Wave Phenomena, Colorado School of Mines, Golden, CO 80401, USA. (agret@mines.edu; rsnieder@mines.edu)

J. Scales, Department of Physics, Colorado School of Mines, Golden, CO 80401, USA. (jscales@mines.edu)